remote sensing

MDPI

Article

Improving the Spatial Accuracy of UAV Platforms Using Direct Georeferencing Methods: An Application for Steep Slopes

Mustafa Zeybek [1,*], Selim Taşkaya [2], Ismail Elkhrachy [3] and Paolo Tarolli [4]

[1] Guneysinir Vocational School, Selcuk University, Konya 42490, Türkiye
[2] Department of Architecture and Urban Planning, Artvin Coruh University, Artvin 08100, Türkiye; selim_taskaya@artvin.edu.tr
[3] Civil Engineering Department, College of Engineering, Najran University, Najran 55461, Saudi Arabia; iaelkhrachy@nu.edu.sa
[4] Department of Land, Environment, Agriculture and Forestry, University of Padova, Viale dell'Università 16, 35020 Legnaro, Italy; paolo.tarolli@unipd.it
* Correspondence: mzeybek@selcuk.edu.tr

Abstract: The spatial accuracy of unmanned aerial vehicles (UAVs) and the images they capture play a crucial role in the mapping process. Researchers are exploring solutions that use image-based techniques such as structure from motion (SfM) to produce topographic maps using UAVs while accessing locations with extremely high accuracy and minimal surface measurements. Advancements in technology have enabled real-time kinematic (RTK) to increase positional accuracy to 1–3 times the ground sampling distance (GSD). This paper focuses on post-processing kinematic (PPK) of positional accuracy to achieve a GSD or better. To achieve this, precise satellite orbits, clock information, and UAV global navigation satellite system observation files are utilized to calculate the camera positions with the highest positional accuracy. RTK/PPK analysis is conducted to improve the positional accuracies obtained from different flight patterns and altitudes. Data are collected at altitudes of 80 and 120 meters, resulting in GSD values of 1.87 cm/px and 3.12 cm/px, respectively. The evaluation of ground checkpoints using the proposed PPK methodology with one ground control point demonstrated root mean square error values of 2.3 cm (horizontal, nadiral) and 2.4 cm (vertical, nadiral) at an altitude of 80 m, and 1.4 cm (horizontal, oblique) and 3.2 cm (vertical, terrain-following) at an altitude of 120 m. These results suggest that the proposed methodology can achieve high positional accuracy for UAV image georeferencing. The main contribution of this paper is to evaluate the PPK approach to achieve high positional accuracy with unmanned aerial vehicles and assess the effect of different flight patterns and altitudes on the accuracy of the resulting topographic maps.

Keywords: UAV; direct georeferencing; GNSS; RTK; PPK; checkpoint; ground control point; accuracy assessment

Citation: Zeybek, M.; Taşkaya, S.; Elkhrachy, I.; Tarolli, P. Improving the Spatial Accuracy of UAV Platforms Using Direct Georeferencing Methods: An Application for Steep Slopes. *Remote Sens.* **2023**, *15*, 2700. https://doi.org/10.3390/rs15102700

Academic Editor: Shawn C. Kefauver

Received: 8 March 2023
Revised: 1 May 2023
Accepted: 20 May 2023
Published: 22 May 2023

1. Introduction

Today, unmanned aerial vehicles (UAVs) are widely used as a tool for mapping and modeling the Earth for various disciplines [1]. UAVs, also known as unmanned aerial systems (UAS) or remotely piloted aircraft systems (RPAS), are pilotless aircraft that can be operated remotely [2,3]. They offer the capability to collect various types of topographical information [4], making them a useful tool in many applications [5–7]. They can be equipped with various sensors, including an Inertial Measurement Unit (IMU) and Global Navigation Satellite System (GNSS) [8]. UAVs have proven to be an effective solution for map production and three-dimensional (3D) recording of terrain [9–11]. A UAV equipped with a camera can capture high-resolution two-dimensional (2D) images of a large area in a single flight and process them through a structure-from-motion (SfM) algorithm to convert them into 3D data and maps [12]. Compared to traditional photogrammetry, SfM provides a more efficient and cost-effective solution for reconstructing 3D models of a

scene. By automatically estimating the camera parameters and positions from the images, SfM eliminates the need for manual measurement, which can be time-consuming and expensive [13–15]. The SfM process produces orthomosaics and digital surface models (DSM) with a resolution of several centimeters from UAV data [16]. Integrating UAV systems and SfM techniques provides a simple and cost-effective way to produce more detailed and accurate maps of terrain [17]. However, the differences between the products produced by the various software packages are not well explored and only a limited number of studies have investigated these differences [18].

UAVs use autonomous flight with GNSS/INS for image capture and landing based on a predefined plan. Recent advancements in direct positioning techniques have improved accuracy to the centimeter level, now integrated into UAV systems. However, direct positioning using only UAV GNSS is limited, requiring measurements of known points. Post-processing kinematic (PPK) improves accuracy and enables direct georeferencing for more accurate map production [19].

The georeferencing of airborne data is possible using high-precision sensors, and it is also cost-effective and uses low-cost GNSS systems. Direct positioning techniques include RTK and PPK. Although RTK requires a radio link, modern UAVs have integrated equipment. PPK systems are reliable for overcoming disruptions and GNSS signal blocks in various applications [20].

Recent studies have focused on using dual-frequency GNSS sensors for direct georeferencing with UAVs. Although commercial software for PPK purposes is being developed, it requires an additional cost. Despite this, there is potential for future advancements in direct georeferencing with UAVs [21,22]. One study [22] examined the accuracy of UAV trajectory positions using low-cost GNSS data and found substantial improvements. Another study [23] explored the potential of UAVs to meet the mapping standards set by the American Society for Photogrammetry and Remote Sensing (ASPRS). A study by Agüera et al. [24] examined the impact of GCPs on the accuracy of DSM and orthophotos produced from UAV photogrammetry. The results suggested that using 15 GCPs measured using traditional technologies such as GPS or tachymetry did not cause a significant loss of accuracy. The study concluded that a map scale of 1:150 with a contour interval of 15 cm could be estimated from 15 GCPs and a flight altitude of 120 m, which is in line with ASPRS mapping standards.

The accuracy of UAV photogrammetry depends on factors such as the GCP number and distribution, image quality, and network geometry. James et al. [25] reported that a well-designed GCP configuration can enhance measurement accuracy and reduce the number of GCPs required. Elkhrachy et al. [26] evaluated the accuracy of four GCP configurations using various software packages. RMSE was used to assess the control points, and the model met the ASPRS 2015 accuracy standards for digital geospatial data. The authors achieved horizontal RMSE values of 4–6 cm and vertical accuracies of 5–6 cm, which were roughly two and three times the ground sampling distance, respectively.

Izuka et al. [27] applied a PPK approach to 3D model reconstruction to reduce the number of required GNSS points. They achieved a high-accuracy model with X, Y, and Z RMSE values of 3.4 cm, 4.9 cm, and 8.0 cm, respectively. The proposed PPK + GCP method enhances measurement efficiency and is a viable alternative to the traditional GCP method, especially in challenging environments.

Liu et al. [28] evaluated the precision of direct georeferencing for UAVs equipped with GNSS and analyzed the impact of GCP quantity and arrangement on system accuracy. They found that as the number of GCPs increased, the RMSE values gradually decreased up to a certain density, with a vertical RMSE value of 8.7 cm and a horizontal RMSE value of 4.1 cm. Optimal accuracy was achieved by evenly distributing the GCPs throughout the study area, with at least one GCP near the area center. Additionally, the study revealed that as the flight height increased, the local accuracy of the DSM decreased.

Rolando et al. [29] showed that using a PPK approach with at least one GCP could result in accurate urban maps at a scale of 1:500, with RMSE values of 3.9 cm, 1.2 cm,

and 3.4 cm for the X, Y, and Z axes, respectively. A study by Cirillo et al. [30] revealed that remote sensing techniques using UAVs offer consistent 3D data with few ground control points, enabling precise characterization of the tectonic evolution of the studied area. Nesbit's study [17] found that direct georeferencing using RTK datasets without the inclusion of GCPs only resulted in slight improvements, and a single GCP was not found to provide reliable results. Belloni et al. [21] showed the potential of UAV-based imagery in monitoring glacier morphology, particularly in challenging fieldwork situations. These studies demonstrate the effectiveness of UAV-based remote sensing techniques in various applications, such as urban mapping, geology, and glacier monitoring. UAVs with SfM–MVS are a high-accuracy alternative for digital measurements. RTK/PPK provides efficient high-accuracy positional data for large areas. It plays a crucial role in surveys conducted in challenging terrains. Although there are limitations in its accuracy assessment, reliable results can be achieved without GCPs using proper camera locations, pre-calibration, and one GCP.

This study aims to determine the optimal achievable accuracy of UAV observations with minimal ground surface surveys. It investigates three different georeferencing techniques for the 3D sparse point-cloud reconstruction of natural and man-made terrain features. The evaluation of UAV-based mapping accuracy is conducted in three stages and is analyzed based on the flight altitude and pattern in a partially forested and steep-slope terrain. The proposed methodology significantly improves the camera location and checkpoint accuracy compared to traditional methods. This study addresses under-researched topics and provides a comprehensive statistical analysis of UAV-based mapping accuracy.

2. Materials and Methods

2.1. Study Area

This research is focused on the Seyitler Campus of Artvin Coruh University, which is situated in the Merkez district of Artvin province, Türkiye (as shown in Figure 1). The study area has approximate WGS84 coordinates of 41.203651077N and 41.834879474E and covers an area of approximately 0.094 km^2. It is mountainous and partially forested terrain, with an elevation range of 879.616 m to 951.583 m, and features hilly landscapes and green areas.

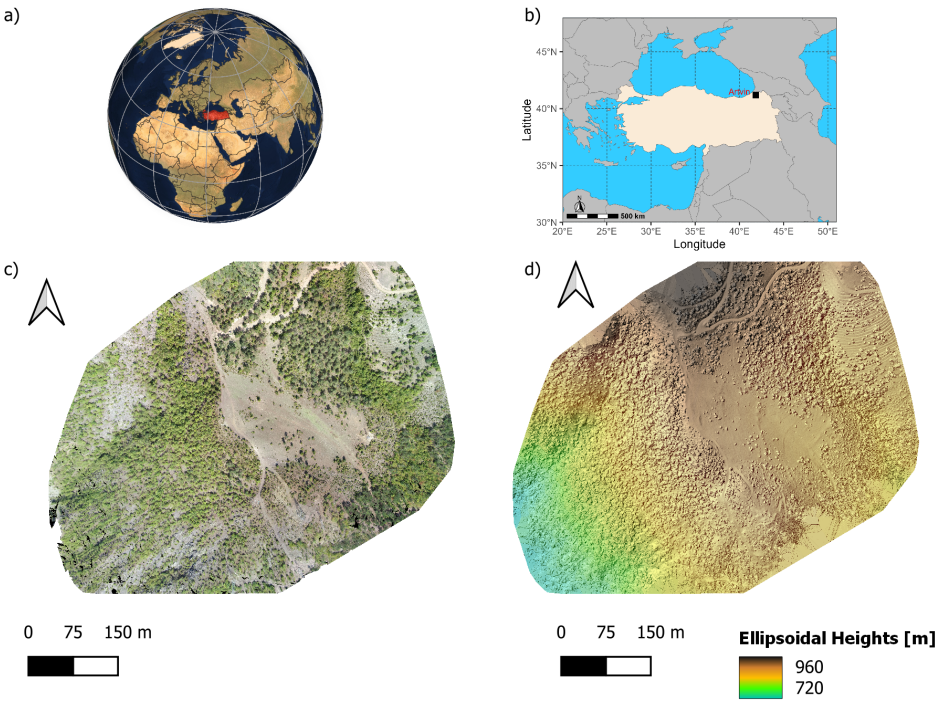

Figure 1. The study area, (**a**) Türkiye in the global sphere, (**b**) the province of Artvin in Turkey, (**c**) the orthomosaics of the study area, (**d**) the DSM of the study area.

2.2. Methodology

This study's workflow is shown in Figure 2 and consists of four main steps as outlined below:

1. Mission planning (field survey, pre-flight and flight parameter settings);
2. Data collection (ground control and checkpoint placement and survey, UAV image acquisition, camera calibration, 1-s Continuously Operating Reference Station-Türkiye (CORS-TR) data);
3. Data processing based on various techniques (bundle block adjustment and image-based matching, RTK and PPK data processing);
4. Horizontal and vertical accuracy evaluation (data and error analysis, evaluation of camera and checkpoint (CP) coordinate differences).

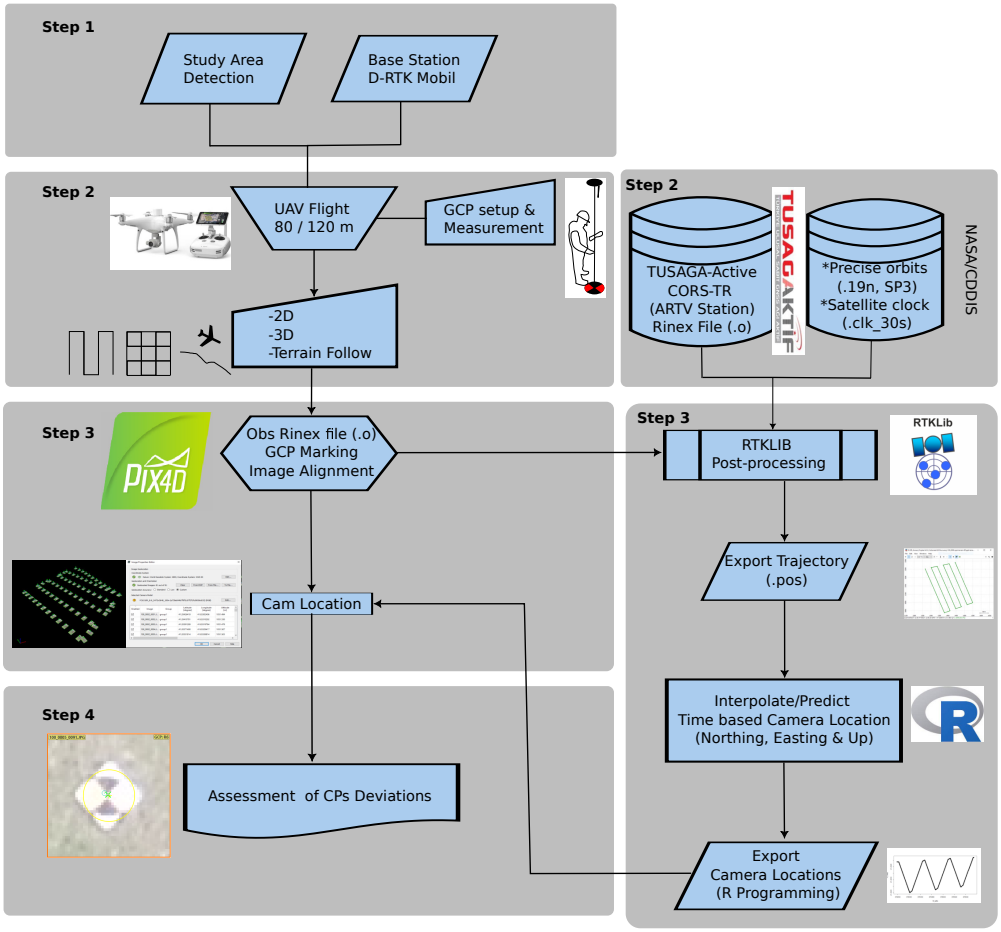

Figure 2. Flowchart of the proposed methodology.

2.3. Data Collection

In this study, data collection was conducted using the DJI Phantom 4 RTK multi-rotor UAV. The DJI Phantom 4 RTK UAV comprises a fuselage, power motors, propellers, a fixed RTK antenna, an autopilot, and a remote ground control unit. The UAV is equipped with a 20-megapixel camera that offers high-resolution imagery, with a GSD of 3.29 cm/pixel and 2.19 cm/pixel at altitudes of 120 m and 80 m, respectively. The images captured by the camera are stored in JPG format on an SD card. Additionally, GNSS observation files and a timestamp file of the image capture time are also included in the Receiver Independent Exchange (RINEX) format.

The UAV and camera used in this study are described in detail in the publication by Zeybek [31]. Information about the image sets collected and the resulting GSD is presented in Table 1. In order to obtain comprehensive data, three types of flights were

conducted during the study, including nadir grid (2D flight), oblique (3D flight), and terrain-following, as shown in Figure 3. The flight planning was carried out using the GSRTK mobile application. The survey area was imported into the ground control remote in KML format to ensure consistency in the flight paths and to enable all flights to cover the same area. To acquire the oblique 3D images, the camera was angled at −30 degrees, creating a unique double-grid pattern.

The study area of 9.4313 ha was surveyed using the DJI Phantom 4 RTK multi-rotor UAV. Due to the low flight altitude and double-grid flight itinerary, an 80 m 3D oblique flight was not performed, and the battery could not be used effectively. The image overlap ratios were set at 80% along the flight path and 70% across the flight path to ensure sufficient data coverage. All flight planning and programming were performed using the DJI GS RTK DJI Ground Station RTK Mobile App (DJI GS RTK App: v2.0.4). The flights were conducted on 27 September 2019 and the Julian Day Number was calculated as 270. For each type of flight, a separate project was created in the Pix4D Mapper software for processing the captured images.

Table 1. The calculated mean ground sampling distance (GSD) values obtained using SfM-based software, which varied depending on the flight height and type (i.e., nadir, oblique, or terrain-following).

	Flight Height	
Capture Mode	**80 m**	**120 m**
RTK/PPK 2D	3.42	4.66
RTK/PPK 3D	NA	6.50
(RTK/PPK) Terrain-Following	1.87	3.12

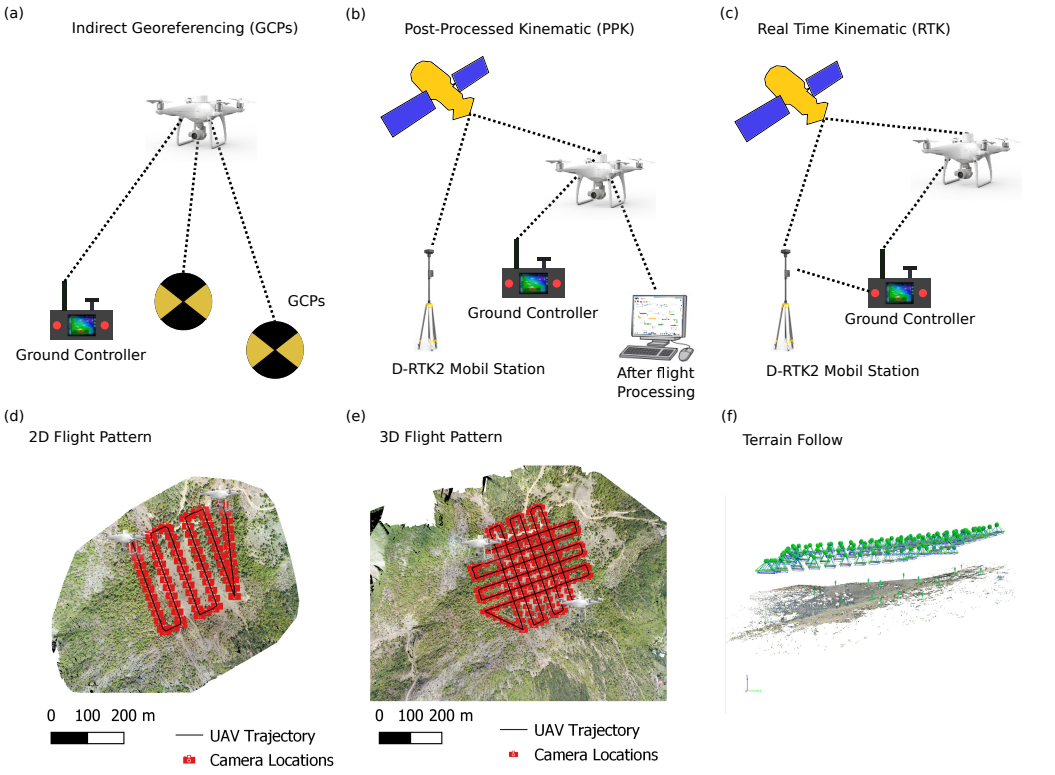

Figure 3. Data processing and flight types: (**a**) indirect georeferencing with GCPs, (**b**) post-processing kinematic (PPK), (**c**) real-time kinematic (RTK), (**d**) nadir 2D flight type, (**e**) oblique 3D flight type, (**f**) terrain-following 2D flight type.

The obtained GSD values were evaluated based on the 2015 ASPRS standards and were found to have an approximate GSD range of 2.5 to 5.0 cm. Considering the horizontal accuracy class, the $RMSE_x$ and $RMSE_y$ values were found to be 5.0 cm and the $RMSE_r$ value was found to be 7.1 cm. At the 95% confidence level, the horizontal accuracy was 12.2 cm. A 1:200 scale map was produced in accordance with the 1990 ASPRS standards.

In this study, 16 GCPs were established. The GCPs were painted with black and orange circles on 0.5-m stakes. The three-dimensional coordinates of these targets were collected using a CORS-TR and an Aschtech Promark 500 GNSS receiver. All data were used after being transformed into the TUREF TM42 coordinate system.

The CORS-RTK module has a multi-frequency GNSS receiver for GCP measurements, with a horizontal accuracy of ±10 mm + 1.0 ppm and a vertical accuracy of ±20 mm + 1.0 ppm RMS, as determined by the manufacturer. The nearest base station to the CORS-TR is the 3.27 km Artvin station (Lat: 41.1751, Long: 41.81832). The expected horizontal and vertical errors were approximately 4.7 cm and 5.7 cm, respectively.

The CORS-TR observation file is published hourly and was downloaded from the TUSAGA Active CORS [32] website. The downloaded data were merged and transformed into a single observation file using the TEQC program [33].

2.3.1. Ground Control Points

GCPs play a crucial role in ensuring the accuracy of photogrammetric measurements. They consist of physical markers on the ground that serve as reference points during image processing and the absolute orientation of the model.

GCPs are known for providing high-precision and consistent data, as they are placed directly on the mapped surface. However, their implementation requires more time and effort, as the coordinates of each marker must be measured using GNSS or total station measurements. Given the limitations of GCPs, there has been a recent shift toward the use of PPK or RTK with UAV-integrated GNSS as alternative methods for achieving high accuracy in photogrammetric measurements.

2.3.2. Real-Time Kinematic (RTK)

The measurements were performed using a DJI D-RTK 2 mobile station (DRTK2). This GNSS base station was specifically designed for the DJI Phantom 4 RTK UAV and was used to perform the direct positioning of the UAV. The DRTK2 was installed at a fixed location with known coordinates (486055.949E, 4563295.909N, 931.613 U, EPSG:5258 in the TUREF TM42 projection system), which were determined by the CORS-RTK technique in advance. The DRTK2 continuously sent real-time corrections to improve the UAV's current coordinate data, ensuring the accuracy and consistency of the measurements. It was important to place the DRTK2 in an area with clear radio frequency communication to prevent interruption of the corrections being sent.

The RTK method enhances the precision of aerial images captured by UAVs through GNSS-based positioning. This method requires a fixed base station to transmit real-time corrections to the UAV's GNSS receiver in a continuous and synchronous manner. This results in a significant improvement in the accuracy of the UAV's position determination compared to solely relying on GNSS signals. It should be noted that the RTK method is effective, regardless of whether the fixed station is a well-known point or a CORS.

The operating principle of the UAV RTK system is based on the traditional RTK measurement method, which is renowned for its high-accuracy positioning capabilities. The RTK system requires a reference station located at a fixed and known position, which continuously sends real-time corrections to the GNSS signals received by the UAV's flight control unit. These corrections are calculated based on the difference between the known position of the reference station and the uncorrected GNSS signals from the UAV. As the UAV moves, the corrections are continually updated, resulting in much higher positioning accuracy than that achieved using standard GNSS signals alone. The corrected data are

then used to geotag the images with EXIF information and prepare them for processing by the image analysis software.

2.3.3. Post-Processing Kinematic (PPK)

PPK is a technique used to increase the accuracy of UAV-based land surveys, without the need for real-time correction data from a GNSS base station. This is achieved using GNSS reference base station data and sensors on the UAV platform during flight to record satellite signal data and imagery.

In comparison to RTK, PPK eliminates the need for a control point with known physical coordinates on the surface, which can speed up the land-surveying process. However, post-processing of the recorded data can be time-intensive, potentially extending the project timeline. Despite this, the increased accuracy of the final results makes PPK a viable option for more precise land surveying.

For the PPK method, we utilized the Artvin (ARTV) TUSAGA Active Continuously Operating Reference Station-Turkey (CORS-TR) base station, which captured data in a static mode at a single known coordinate per second. The data were recorded for one hour, processed using the TEQC program [33], and consolidated into a single file for use with all flight data. The day was set to the 270th day of the year with a start time of 07:59 (GMT+2). A broadcast navigation file was also necessary so NASA's daily GPS broadcast ephemeris data were obtained from the CDDIS website [34]. In addition, the clock data were downloaded from another International GNSS Service (IGS) site and utilized in the calculations as an SP3 file. It is important to note that the final, most consistent, and highest-quality IGS solutions are typically obtained from weekly orbit files generated approximately 13 days after the solution week has ended. All operational IGS GNSS products (i.e., orbits, station positions, Earth orientation parameters, clock solutions) are organized and stored in subdirectories based on the GPS week.

To perform the analysis of the PPK flights, separate projects were created in the Pix4DMapper software specifically for PPK while maintaining consistency in GCP tagging by duplicating the projects created for RTK. The processing of GNSS data and the camera positioning calculation required the use of third-party software. The DJI Phantom 4 RTK (P4RTK) UAV captured Receiver Independent Exchange Format (RINEX) data for all flights and recorded the time of capture. The GNSS data were processed using the free RTKLIB software to geolocate the camera positions, utilizing the GNSS RINEX *obs* files stored on the P4RTK's SD card. The 1 s ARTV CORS-TR GNSS points and the UAV observation files were processed using this software.

The first step in PPK processing was the subsequent processing of the flight GNSS data, which was facilitated by the use of data derived from the ARTV CORS station. The RTKLIB software package, which performed all the necessary calculations for the PPK processing, also displayed the standard deviation of the calculated solution to control the quality of the data processing stage. This step was carried out using the RTKLIB (version 2.4.3) demo5 b34g open source solution. This toolbox was prepared by Tomoji Takasu at the Tokyo University of Marine Science and Technology [35].

The UAV's GNSS measurement unit has a measurement capacity of 5 Hz [6]. The UAV speed is 5 m/s, and in this case, the camera position requires an estimate every 1 m. Interpolation is required to find the intermediate values. To obtain more accurate results, a loess model was created between the time and coordinate values using the R *loess* function [36,37]. A 1D interpolation model was created for time and each axis (northing, easting, and up).

In the R programming language [37], the locally weighted scatterplot smoothing (loess) function was used to apply a local regression model. The resulting model is determined by nonparametric regression using locally weighted regression [38]. This technique models the data within small neighborhoods and is based on a series of polynomial regressions [39].

The regression analysis using the loess model is a powerful tool for identifying patterns in scattered data points. It is a form of local polynomial smoothing that adjusts the bandwidth of estimation based on the smoothing parameter [40,41]. The span, which is the fraction of data used for estimation at each point, is a key factor that determines the accuracy of the results. This method is particularly well-suited for large datasets, making it an ideal tool for data analysis.

Using a smoothing function $g(x)$ and a random error with a mean of 0 and constant variance, the response variable Y is generated as follows:

$$Y_i = g(x_i) + \epsilon \quad (1)$$

For each observation (i) at x, a polynomial is estimated using a smoothing parameter. The degree of the polynomial and the smoothing parameter provide the user with a choice based on error minimization.

This model was chosen primarily because it provides a regression that can be used as a line or higher-degree polynomial, and it requires a smoothed estimate when determining the camera-shot position of the UAV GNSS point. The choice of a local regression rather than a standard regression is due to the fact that only a relatively small number of points are used in the vicinity of the camera-shot point on either side. The use of weighting reduces the influence of points outside the immediate vicinity, resulting in robust regression.

In order to eliminate systematic errors, the addition of a GCP to the PPK results (PPK1) allows for higher positional accuracy (Figure 4). Another aspect of the analysis is a comparison with the results obtained using commercial PPK software. This software is the widely used Topodrone TOPOSETTER P4RTK v1.0 (Soft.) software.

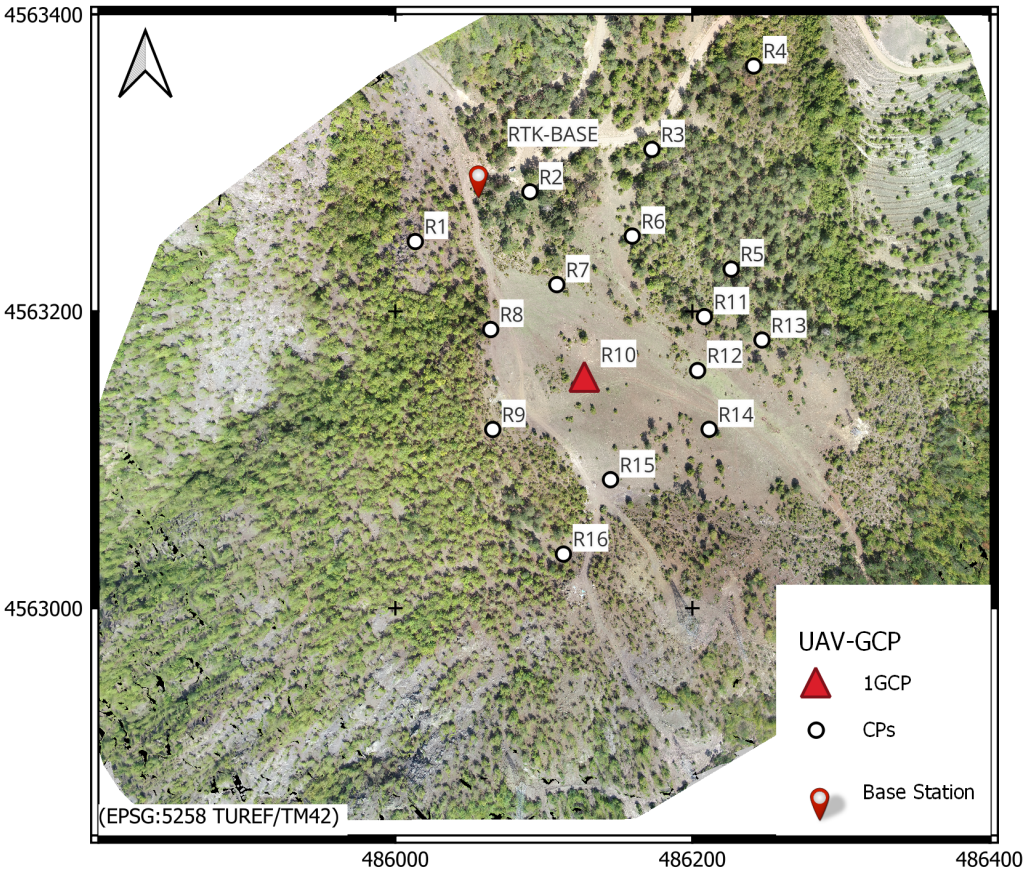

Figure 4. 1 GCP (R10)'s location and distribution of other checkpoints.

2.4. Image Processing

The image processing in this study was carried out using Pix4DMapper software, version 4.5.6, which is a well-established software package known for its use of SfM techniques. Pix4DMapper can import camera positions from multiple sources, including EXIF data and external files in csv or txt formats. The software is equipped with several camera-related functions such as BBA, camera calibration, GCP tagging, and optimization. The evaluation in this study focused on the camera positions and control points, so a sparse point-cloud generation was deemed sufficient. As a result, the image processing procedure was divided into three sequential steps.

The first step is to align the images by describing and matching the features in the images. In the second step, if pre-calibration has been performed, these calibration parameters should be entered and the conditions of the parameters should be specified in the settings section to ensure that certain rates are not exceeded in the optimization step. Otherwise, large changes in the parameters may occur.

To ensure optimal results, it is important to perform camera calibration procedures if the camera has not already been calibrated. Camera calibration is a process that enables the estimation of the internal orientation of a camera and the correction of lens distortion parameters. Various techniques have been developed for this purpose, including self-calibration and field calibration. In this study, we utilized the self-calibration method for camera calibration. To achieve this, we used a reference site with ground control points for the adjustment of aerial photographs [31]. The next step is to identify and mark the locations of the GCPs or CPs in at least three images. These markers serve to improve the camera positioning and enhance the accuracy of the SfM project by including at least three GCP definitions. If quality control of the project is necessary, it is imperative to assign CPs.

By comparing the real and BBA estimates and determining the point position errors, this process allows for a thorough spatial evaluation of the project. Upon completion of these steps, the camera position for each image, the internal camera parameters, and the 3D coordinates of the sparse point cloud of the terrain are obtained.

2.5. Accuracy Assessment

The descriptive statistics given in Equations (2)–(5) were used to assess both the horizontal and vertical accuracy. Accuracy was evaluated by calculating the RMSE of the differences between the GCP coordinates measured using the 3D model (BBA) and the on-site dual-frequency GNSS. The radial horizontal accuracy, $RMSE_r$, including both x and y coordinate errors, and the vertical accuracy, $RMSE_Z$ (z), were determined based on the parameters derived from the Pix4D project.

$$RMSE_X = \pm\sqrt{\frac{\sum_{i=1}^{n}(X_E - X_{GNSS})^2}{n}} \tag{2}$$

$$RMSE_Y = \pm\sqrt{\frac{\sum_{i=1}^{n}(Y_E - Y_{GNSS})^2}{n}} \tag{3}$$

$$RMSE_Z = \pm\sqrt{\frac{\sum_{i=1}^{n}(Z_E - Z_{GNSS})^2}{n}} \tag{4}$$

$$RMSE_r = \pm\sqrt{RMSE_X^2 + RMSE_Y^2} \tag{5}$$

In the given equations, X_E, Y_E, Z_E are the estimated coordinate values after UAV data processing (BBA); $X_{GNSS}, Y_{GNSS}, Z_{GNSS}$ are the coordinate values obtained by the GNSS receiver in the field; and n is the number of points. If the RMSE values are evaluated separately for the horizontal and vertical axes, the analysis of the $RMSE_r$ and $RMSE_Z$ values is more accurate.

3. Results

The results of the applied techniques were evaluated using the RMSE values. The validity of the implementation of the ASPRS 2015 standards was confirmed through the evaluations. Table 2 presents the results of the SfM with 16 GCPs and it is evident that the best results were obtained using the PPK + 1 GCP method. When comparing the different methods, it can be seen that the horizontal positional accuracy ($RMSE_r$) was higher for PPK than RTK. On the other hand, the RTK solution showed better accuracy in the vertical component. The proposed method of adding 1 GCP to PPK provided the best positional results.

Table 2. RMSE values for CPs.

Method	Altitude	$RMSE_r$ (m)	$RMSE_Z$ (m)
RTK 2D	80 m	0.038	0.039
	120 m	0.044	0.046
PPK 2D	80 m	0.033	0.059
	120 m	0.031	0.062
PPK1 2D	80 m	**0.023** *	**0.024** *
	120 m	0.019	0.033
PPK Soft. 2D	80 m	0.033	0.157
	120 m	0.032	0.073
RTK 3D	80 m	-	-
	120 m	0.044	0.115
PPK 3D	80 m	-	-
	120 m	0.020	0.130
PPK1 3D	80 m	-	-
	120 m	**0.014** **	0.088
PPK Soft. 3D	80 m	-	-
	120 m	0.026	0.046
RTK Terrain-Following	80 m	0.045	0.047
	120 m	0.040	0.050
PPK Terrain-Following	80 m	0.030	0.096
	120 m	0.045	0.094
PPK1 Terrain-Following	80 m	0.024	0.025
	120 m	0.035	**0.032** **
PPK Soft. Terrain-Following	80 m	0.033	0.181
	120 m	0.040	0.050

* The smallest RMSE values for 80 m. ** The smallest RMSE values for 120 m.

When evaluated by flight type, the values were similar. For example, in Table 2, it can be seen that the RTK 2D and RTK terrain-following values appear to be similar. Based on the assessment of the differences between RTK and PPK, it was found that PPK produced better solutions than RTK in terms of the horizontal components, as indicated by the lower $RMSE_r$. However, in terms of the vertical component, $RMSE_Z$, RTK produced solutions with relatively higher accuracy than PPK. The reason for the observed differences in the vertical component is believed to be due to the fact that RTK uses instantaneous corrections with high-frequency 5 Hz data, whereas PPK relies on 1 Hz data provided by the CORS-TR station. This suggests that the frequency of data used for corrections could play a significant role in determining the accuracy of the vertical component in positioning. In cases where high accuracy is required, it may be necessary to eliminate systematic errors using GCPs. Adding GCPs can help to improve the accuracy of the positioning by identifying and correcting systematic errors in the data. In the case mentioned, the addition of one GCP resulted in improvements in the accuracy of the positioning. This suggests that there may have been a systematic error present in the data that was corrected by the addition of the GCP. It is important to note that the number and placement of GCPs required for accurate positioning will depend on the specific application and level of accuracy required.

The residuals of the camera positions based on PPK and the 16 marked GCPs are shown in Figures A1–A5. Additionally, these figures depict the results of the analysis and whether the residuals were normally distributed. They also allow for an examination of the minimum, maximum, and density of errors and can be used to investigate the causes of inaccurate points and sources. In particular, the sharpness at the turning points of the camera positions led to increased position differences. The term "GCP" refers to the adjusted camera positions in the project marked with PPK + 16 GCPs. These figures show the comparison results of the different methods used to determine camera positions in a photogrammetry or remote sensing project. These methods include RTK, PPK, and PPK + 1 GCP (post-processing kinematic with one ground control point).

In Figure A1, it can be seen that the camera positions with the best residual of −0.02 to 0.04 m were obtained using PPK + 1 GCP. The RTK solution also showed that some points have a different position during the adjustment phase. The distributions of the CPs (control points) were found to be normal. The PPK + 1 GCP values ranged from −0.04 to 0.08 m.

Figure A2 shows that the differences in the camera positions were obtained in the range of 0.025 to 0.075 for PPK + 1 GCP. Although the data deviated from a normal distribution, the accuracy of the data is more important. Systematic errors are easier to minimize in this case. Here, however, random errors rather than systematic errors occurred between the methods. The CPs showed a normal distribution. The residuals were obtained with PPK + 1 GCP in the range of −0.05 to 0.05 m.

In Figure A3, it can be seen that the camera positions were in the range of −0.016 to 0.00 m. The RTK residuals were within a normal distribution. The CPs had residuals ranging from −0.04 to 0.02 m with PPK + 1 GCP. The CP residuals showed a normal distribution.

In Figure A4, it can be seen that the camera positions were in the range of −0.12 to 0.00 m for PPK + 1 GCP. The camera positions were generally not within a normal distribution. The PPK solution had residuals of a few meters. We can see that the addition of the GCP made an important correction to the camera positions. The commercial software produced very good results here. PPK + 1 GCP had residuals in the range of −0.12 to 0.00 m. The residuals of the CPs showed a normal distribution.

In Figure A5, it can be seen that the camera positions were in the range of −0.05 to 0.10 m for PPK + 1 GCP. The non-RTK methods had residuals that were not within a normal distribution. The CPs had residuals in the range of −0.06 to 0.06 m. The residual distributions of the CPs showed a normal distribution.

3.1. Accuracy of RTK Ground Control Points

The RMSE values were evaluated based on the number of errors in each of the GCPs in the project. Different solutions were tested based on the type of flight (2D: nadir flight; 3D: oblique flight and terrain-following) and the height of the images obtained in the field. These tests involved using a reference GNSS receiver connected to a CORS-TR survey point close to the field survey and a UAV system connected to the DRTK2. The images were corrected in real time using the measured values of each GCP in the field. The RTK evaluation tested the accuracy of the project by using all points as CPs without any GCPs. In addition to these evaluations, the projects were also evaluated according to ASPRS standards and classifications.

For RTK 2D 80 m, according to a GSD of 3.42 cm/px and a horizontal accuracy class of 5 cm, the $RMSE_r$ value should be 7.1 cm. Looking at Table 2, this value was 3.8 cm, which means it was well within the ASPRS limits. The vertical accuracy $RMSE_Z$ was 3.9 cm and the ASPRS vertical accuracy class was 5 cm.

The RTK 2D pattern GSD typically has a resolution of 4.66 cm/px for an altitude of 120 m, which corresponds to a horizontal accuracy class of 5 cm and an $RMSE_r$ value of 7.1 cm. As seen in Table 2, the $RMSE_r$ value obtained was 4.4 cm, which meets the ASPRS criteria. The vertical accuracy $RMSE_Z$ was 4.6 cm and the vertical accuracy class was 5 cm.

The RTK 3D pattern GSD typically has a resolution of 6.50 cm/px for an altitude of 120 m, which corresponds to a horizontal accuracy class of 7.5 cm and an $RMSE_r$ value of

10.6 cm. According to Table 2, the value obtained for this pattern and altitude was 4.4 cm, which meets the ASPRS criteria. The vertical accuracy $RMSE_Z$ was 11.5 cm and the vertical accuracy class was 15 cm.

The RTK terrain-following pattern GSD typically has a resolution of 1.87 cm/px for an altitude of 80 m and the horizontal accuracy class should be 2.5 cm, with an $RMSE_r$ value of 3.5 cm. According to the values presented in Table 2, it was found to be 4.5 cm. The reason for this higher value compared to the GSD cm/px ratio was investigated and it was found that although the flight plans were minimized to optimize flight time and battery usage, some GCPs were located at the edges, causing the RMSE values to approach 6 cm. However, in the central part of the study area, RMSE values of 1.4 cm were observed. The vertical accuracy $RMSE_Z$ was 4.7 cm and the vertical accuracy class was 5 cm.

For the RTK terrain-following pattern and an altitude of 120 m, the GSD resolution is typically 3.12 cm/px, the horizontal accuracy class is 5 cm, and the $RMSE_r$ value should be 7.1 cm. As shown in Table 2, the value obtained was 4.0 cm, which meets the ASPRS criteria. The vertical accuracy $RMSE_Z$ was 5.0 cm and the vertical accuracy class was 5 cm.

3.2. Accuracy of Post-Processing Kinematic

The camera positions were evaluated using the PPK data and the proposed approach and then processed using the Pix4DMapper software. After processing, the camera positions estimated using the PPK method and the BBA point estimates obtained using the CPs were compared.

The $RMSE_r$ and $RMSE_Z$ values for PPK 2D 80 m and RTK 2D met the ASPRS standards. The camera position RMSE error for PPK 2D 80 m was less than 50% of the RTK 2D values, with X, Y, and Z values of 0.008, 0.008, and 0.009 m respectively. It was found that the positional solutions were better with RTK. The reprojection error for both projects was 0.126 px. The focal length for RTK 2D 80 m was 3658.837 px and 8.581 mm, whereas for PPK 2D 80 m, it was 3658.811 px and 8.581 mm. As the project settings were the same, these differences were caused by the positional solution. The results for PPK 2D 120 m were similar to those for PPK 2D 80 m.

For the PPK Soft. solutions, the results were obtained using commercial software. PPK Soft. 2D 80 m showed significantly lower $RMSE_Z$ results. Upon investigation, it was found that although the RMSE values for the camera positions in PPK 2D 80 m were 0.008, 0.008, and 0.009 m for X, Y, and Z, respectively, the RMSE values for PPK Soft. 2D 80 m were 0.030, 0.013, and 0.157 m for X, Y, and Z, respectively. This indicates that the accuracy of the camera position solutions generated by the software was low. The SfM project parameters were the same. The results for PPK Soft. 2D 120 m had the same horizontal positions as those for PPK Soft. 2D 80 m, but achieved 2 times higher accuracy in the Z axis.

PPK 3D 120 m had high horizontal positional accuracy but low accuracy on the vertical axis. When comparing PPK + 16 GCP, it was found that the project parameters were the same. However, it was observed that the RMSE values for the camera positions in the PPK + 16 GCP project were 0.008, 0.009, and 0.117 m for X, Y, and Z, respectively. The use of GCPs caused significant changes in the camera positions during the BBA phase. PPK Soft. 3D 120 m provided the same horizontal and vertical positional accuracies as RTK 3D 120 m, according to ASPRS standards. In addition, the accuracy level in the Z axis was higher than in RTK 3D 120 m.

PPK terrain-following 80 m met the standards for horizontal positions but the accuracy level in the Z axis was low. The results for PPK terrain-following 120 m were close to those of RTK 3D 120 m for both the horizontal and vertical positional accuracies.

3.3. Accuracy of Post-Processing Kinematic and 1 GCP

In this section, the positional accuracy on the map was further improved by using only 1 GCP in addition to the PPK results. The camera centers were determined using the PPK results and 1 GCP was placed on the part of the terrain corresponding to the center

of the CP (R10) (Figure 4). The Pix4DMapper software facilitated this. This resulted in a significant improvement in positional accuracy, especially in the Z-axis.

When evaluated according to ASPRS 2015, the $RMSE_r$ values obtained ranged from 1.4 cm to 3.5 cm. The horizontal accuracy at the 95% confidence level (cm) corresponded to 6.1 cm, meeting the mapping standard of a 1:100 scale, according to ASPRS 1990. A map with better positional accuracy was produced compared to the GSD comparison. According to the information presented in Table 2, the $RMSE_Z$ values ranged from 2.4 to 8.8 cm for non-vegetation areas (cm), indicating a vertical accuracy class of 10 cm. As a result, the data obtained using the PPK + 1 GCP method provided higher positional accuracy than the RTK method.

4. Discussion

In this study, five projects were evaluated: RTK, PPK, PPK + 1 GCP, PPK + 16 GCP, and PPK Soft. At the same time, a total of 25 projects were produced, considering various flight types, altitudes, control points, and direct geo-referencing techniques, and compared against established standards. The results obtained using the proposed methodology produced RMSE values that met the ASPRS mapping standard. The proposed solutions for RTK and PPK were analyzed in order to investigate the accuracy criteria, even for areas where the topography is variable under difficult conditions. Projects of different heights (80 m and 120 m) and possible different design types were statistically compared.

This study investigated the PPK approach to improve the accuracy of 3D models generated using UAVs. It is known that the precise estimation of camera positions in the geographic coordinate system can be used in bundle adjustment [27]. However, the image capture positions contain some errors when the GNSS-based coordinate information is obtained instantaneously, and by updating the coordinates with PPK using the precise orbit values of satellites, better spatial accuracy can be achieved through better positioning. In addition to improving camera positions, the use of 1 GCP has been shown to eliminate systematic sources of error.

The present study has shown that RTK and PPK systems can be used independently to produce models that meet accuracy criteria. The use of a GCP is essential to further improve these standards. The use of an up-to-date calibration file for the height components is important when GCPs are not used, as deviations in the height components can occur [31].

Taddia et al. [6] reported that the oblique dataset produced very similar results both with GCPs (3D RMSE = 2.5 cm) and without GCPs (3D RMSE = 2.8 cm), whereas the dataset with the lowest accuracy was more affected by the positioning and number of GCPs (3D RMSE ranging from 3.4 to 7.5 cm). Adding some oblique images to the nadir dataset without any GCPs was found to improve the vertical accuracy of the model (RMSE ranging from 5.2 to 2.5 cm) and it was also noted that for P4RTK and PPK, the nadir datasets are a faster solution without GCP than 3D oblique image acquisition. When the RMSE values obtained in the previous study were compared with the values obtained in this study, it can be seen that the results were similar. Therefore, RMSE values can be reduced by either adding 1 GCP to the nadir images or supporting them with oblique images.

The proposed methodology has shown that flights conducted considering the terrain and variations in flight altitude can produce different RMSE values. The use of the freely available RTKLib and R programming packages was found to result in lower RMSE errors compared to commercial software and previously completed research.

The proposed approach offers the possibility of obtaining a reliable and high-accuracy model of small areas in a much shorter time, without the need for intensive coordinate information on the surface, and with a high resolution for surface exploration. However, these solutions require the necessary measurement data, which are typically made available by NASA CDDIS with an approximately 13-day delay.

The accuracy of each point in the UAV mapping depends not only on the scale and resolution of the source image but also on the accuracy of the initial camera position. Flying at lower altitudes can produce small-scale images and smaller GSDs, whereas the accuracy

of GNSS or GCP solutions (both vertical and horizontal) is more relevant to the accuracy of the maps. In this context, surveyors should carefully evaluate RTK/PPK solutions in GNSS positional solutions for higher accuracy and quality, rather than solely considering small GSD and pixel values. In particular, the use of 1 GCP in PPK solutions can increase accuracy. The results of this study can be applied to various fields such as environmental monitoring, forestry, and land management, where high-precision mapping is necessary.

5. Conclusions

This study discusses the potential of the PPK method to improve the accuracy of 3D models produced by recent UAVs. The proposed method was applied to data collected by the DJI Phantom 4 RTK UAV platform due to its widespread use by end users. In nadir flight (2D), the positional accuracy in both the horizontal and vertical axes reached the highest level compared to other measurement techniques and methods, resulting in RMSE values of 2.3 cm and 2.4 cm in the horizontal and vertical axes, respectively, at an altitude of 80 m. In addition, a horizontal plane accuracy of 1.4 cm RMSE was obtained at an altitude of 120 m using an oblique (60-degree) camera. The results show that the PPK and 1 GCP methods can increase measurement efficiency with less survey effort, resulting in a better 3D model. The use of pre-calibrated camera parameters and the proposed PPK configuration can reduce the fieldwork burden for geospatial researchers and practitioners and highlights the need for them to consider these recommendations in future studies. The results clearly demonstrate the advantages of using a UAV to produce high-accuracy orthomosaics and digital terrain models. The accuracy of the results does not differ from that of standard ground measurements, but the time required for data collection and processing is significantly shorter. Therefore, the proposed method provides an alternative approach to GCP that can be adapted to areas where the use of ground control points is not possible such as areas with difficult geological structures, sloping terrain, forest areas, wetlands, and glaciers. The main aim of this study was to investigate the positional accuracy caused by different altitudes and flight patterns, as well as the accuracy criteria obtained using the RTK and PPK methods. Our proposed method achieved the lowest RMSE values in all nadir, oblique, and terrain-following patterns and at both altitudes. Due to the rapid development and miniaturization of GNSS and other electronic systems, there is a significant market demand for RTK-enabled UAV systems. By combining the real-time positional access provided by these technologies with post-processing techniques and the proposed methodology, standards for map production can be significantly improved.

Author Contributions: Conceptualization, M.Z.; Data curation, M.Z.; Formal analysis, M.Z.; Investigation, M.Z.; Methodology, M.Z.; Resources, M.Z.; Software, M.Z.; Supervision, M.Z.; Validation, M.Z., S.T., I.E. and P.T.; Visualization, M.Z.; Writing–review and editing, M.Z., S.T., I.E. and P.T.; Funding Acquisition, P.T. All authors have read and agreed to the published version of the manuscript.

Funding: This research received no external funding.

Data Availability Statement: The data presented in this study are available on request from the corresponding author.

Acknowledgments: The authors would like to express their gratitude to Sefa Yalvaç from Gümüşhane University for his comments on the GNSS technique used during the processing phase of PPK and RTK. Data used in this study were obtained from NASA's CDDIS. We acknowledge the contribution of NASA in making this data publicly available.

Conflicts of Interest: The authors declare no conflict of interest.

Abbreviations

The following abbreviations are used in this manuscript:

2D	two-dimensional
3D	three-dimensional
ARTV	Artvin
ASPRS	American Society for Photogrammetry and Remote Sensing
BBA	bundle block adjustment
CDDIS	Crustal Dynamics Data Information System
CP	checkpoint
CORS-TR	Continuously Operating Reference Station-Türkiye
ÇOMÜ	Çanakkale onsekiz mart üniversitesi
DRTK2	DJI D-RTK 2 mobile station
DSM	digital surface model
EPSG	European petroleum survey group
GCP	ground control point
GCS	ground control station
GMT	Greenwich mean time
GNSS	Global Navigational Satellite Systems
GSD	ground sampling distance
IGS	International GNSS Service
IMU	Inertial Measurement Unit
INS	Inertial Navigation Systems
KML	keyhole markup language
Lat	latitude
Long	longitude
M3C2	multiscale model to model cloud comparison
MVS	multi-view stereo
NASA	National Aeronautics and Space Administration
PPK	post-processing kinematic
PPM	part-per-million
RINEX	Receiver Independent Exchange Format
RMSE	root mean square error
RPAS	remotely piloted aircraft systems
RTK	real-time kinematic
SfM	structure from motion
TM	transverse mercator
TUREF	Turkish national reference frame
UAS	unmanned aerial system
UAV	unmanned aerial vehicle

Appendix A

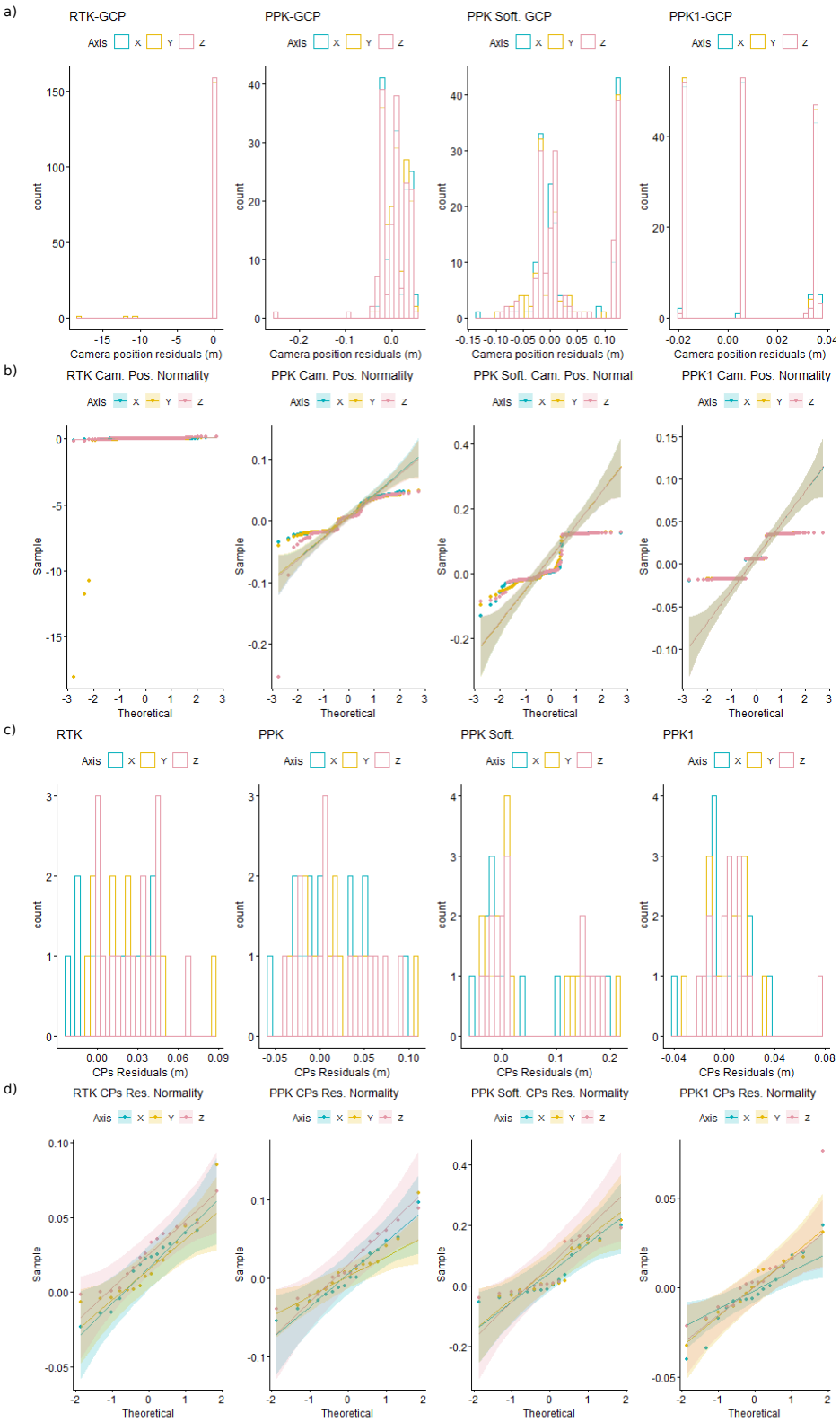

Figure A1. Results of 80 m 2D flight: (**a**) estimated camera position residual histograms, (**b**) camera position normality, (**c**) CP residuals, (**d**) CP residual normality plots.

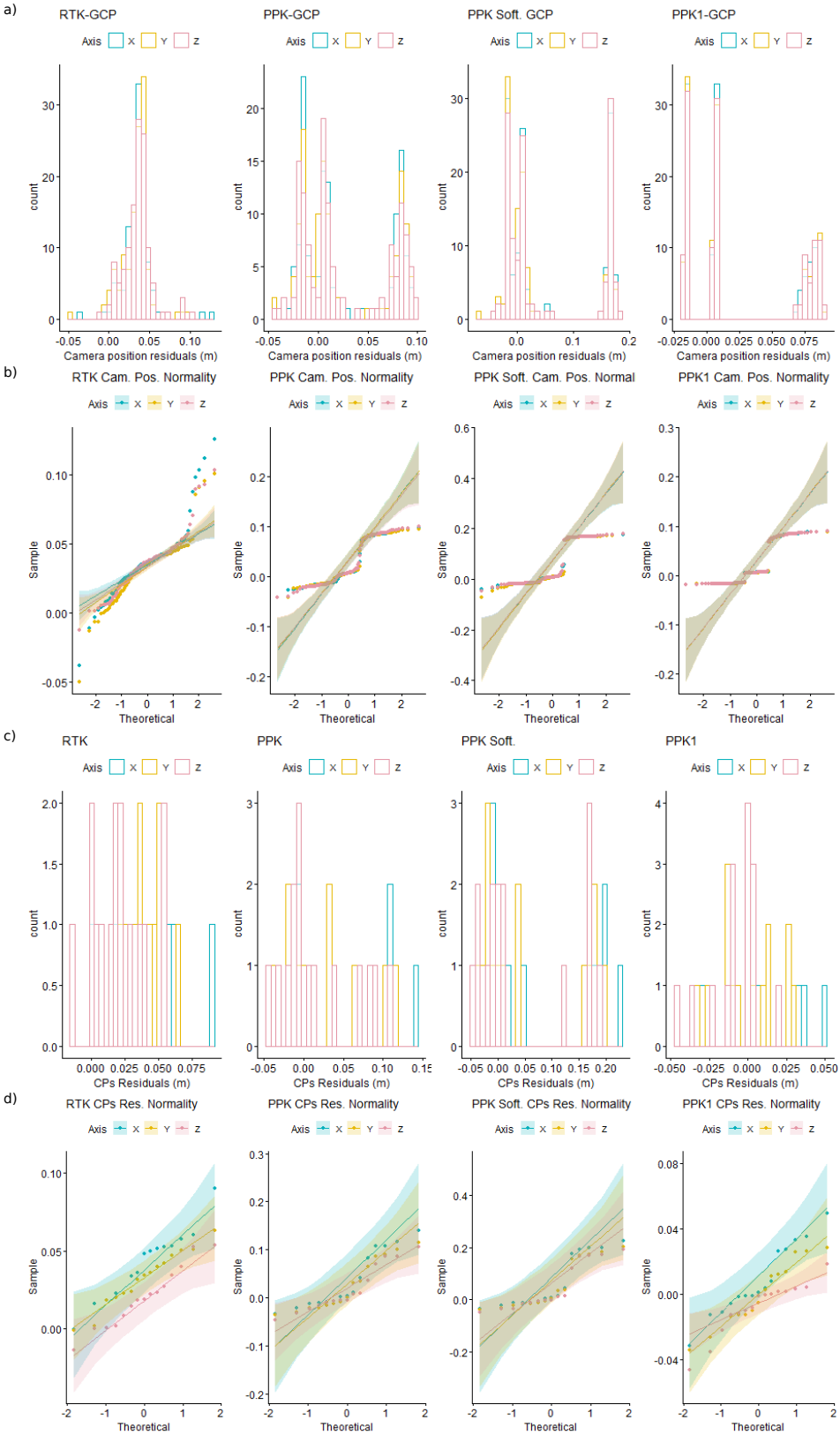

Figure A2. Results of 80 m terrain-following flight: (**a**) estimated camera position residual histograms, (**b**) camera position normality, (**c**) CP residuals, (**d**) CP residual normality plots.

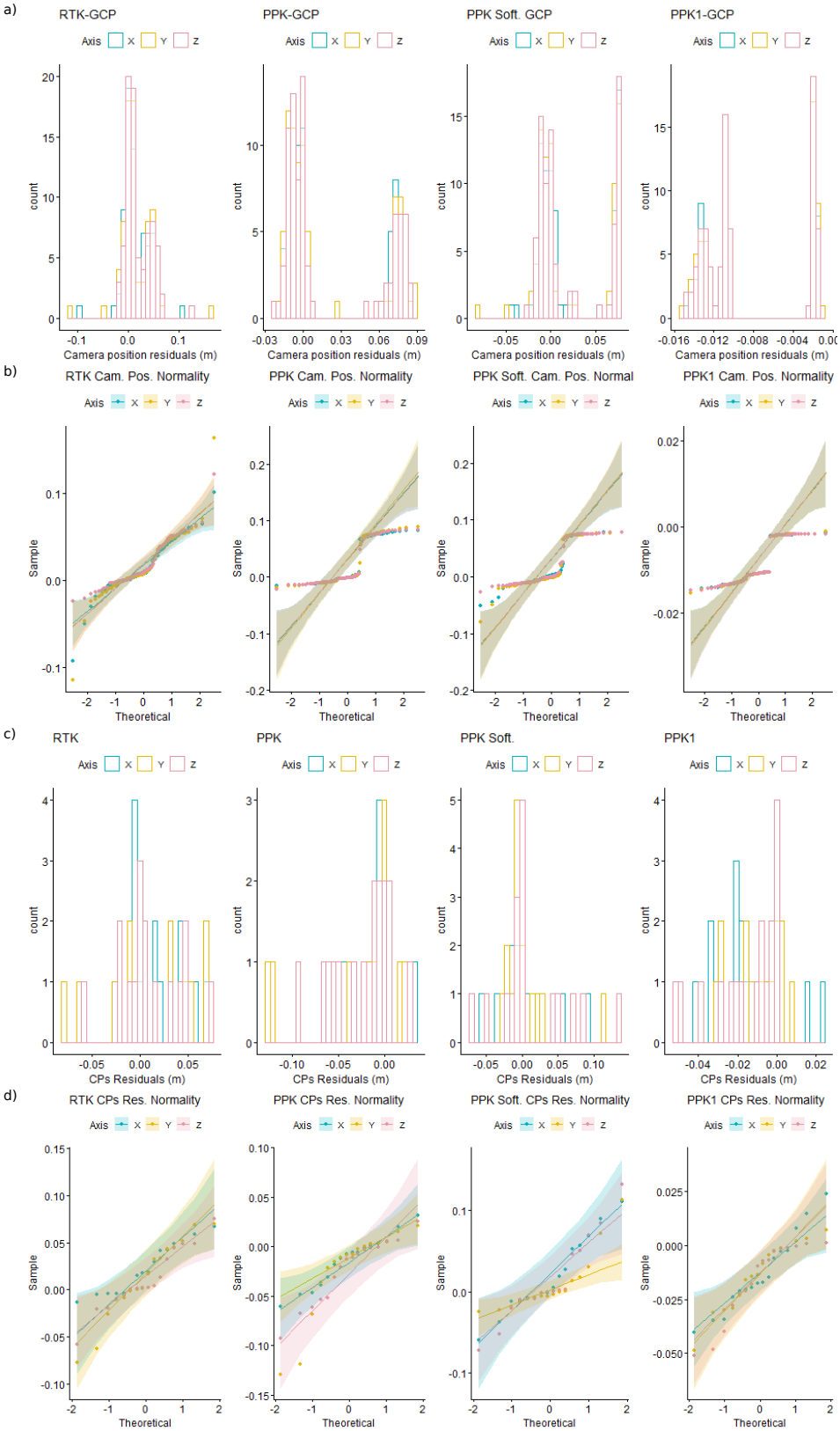

Figure A3. Results of 120 m 2D flight: (**a**) estimated camera position residual histograms, (**b**) camera position normality, (**c**) CP residuals, (**d**) CP residual normality plots.

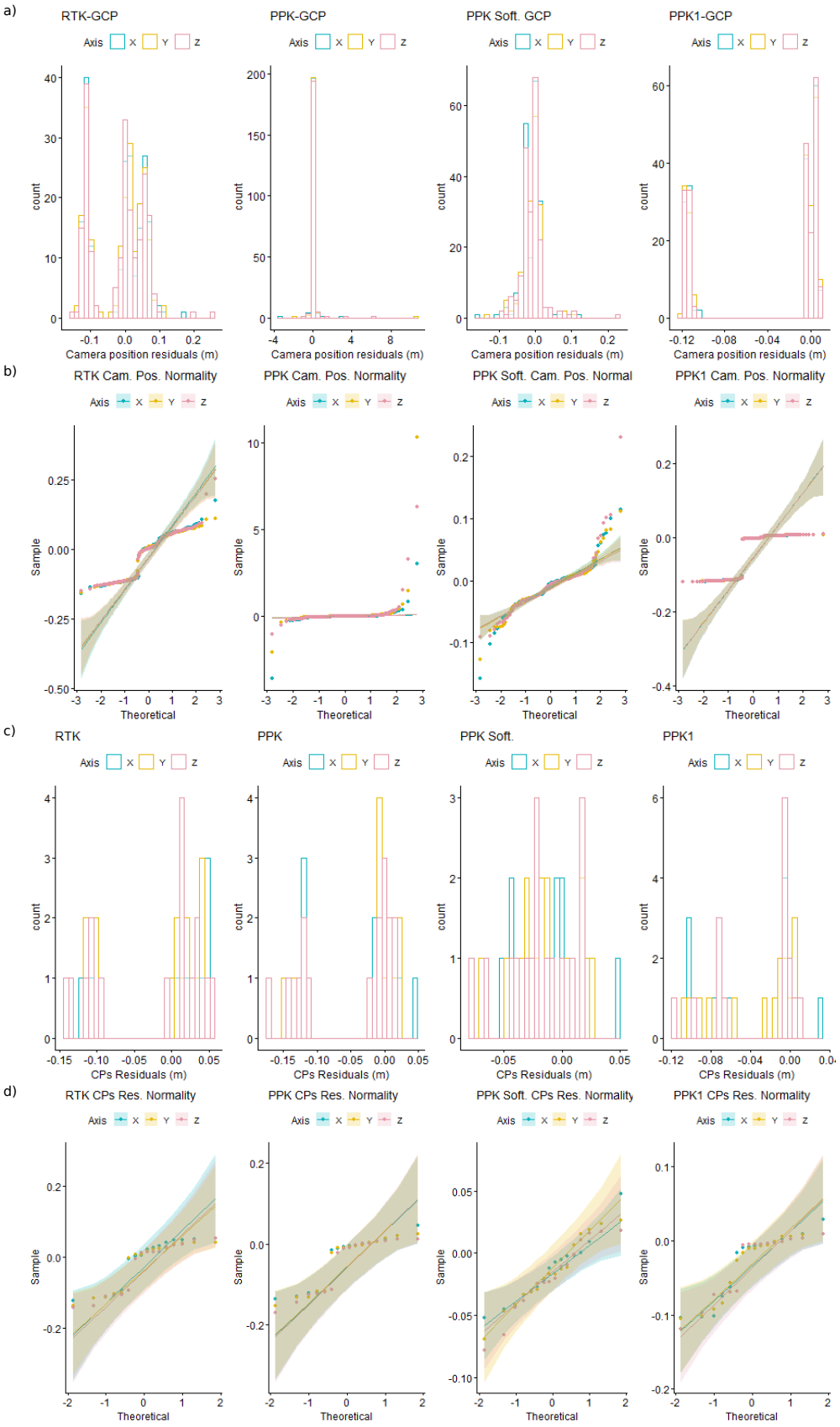

Figure A4. Results of 120 m 3D flight: (**a**) estimated camera position residual histograms, (**b**) camera position normality, (**c**) CP residuals, (**d**) CP residual normality plots.

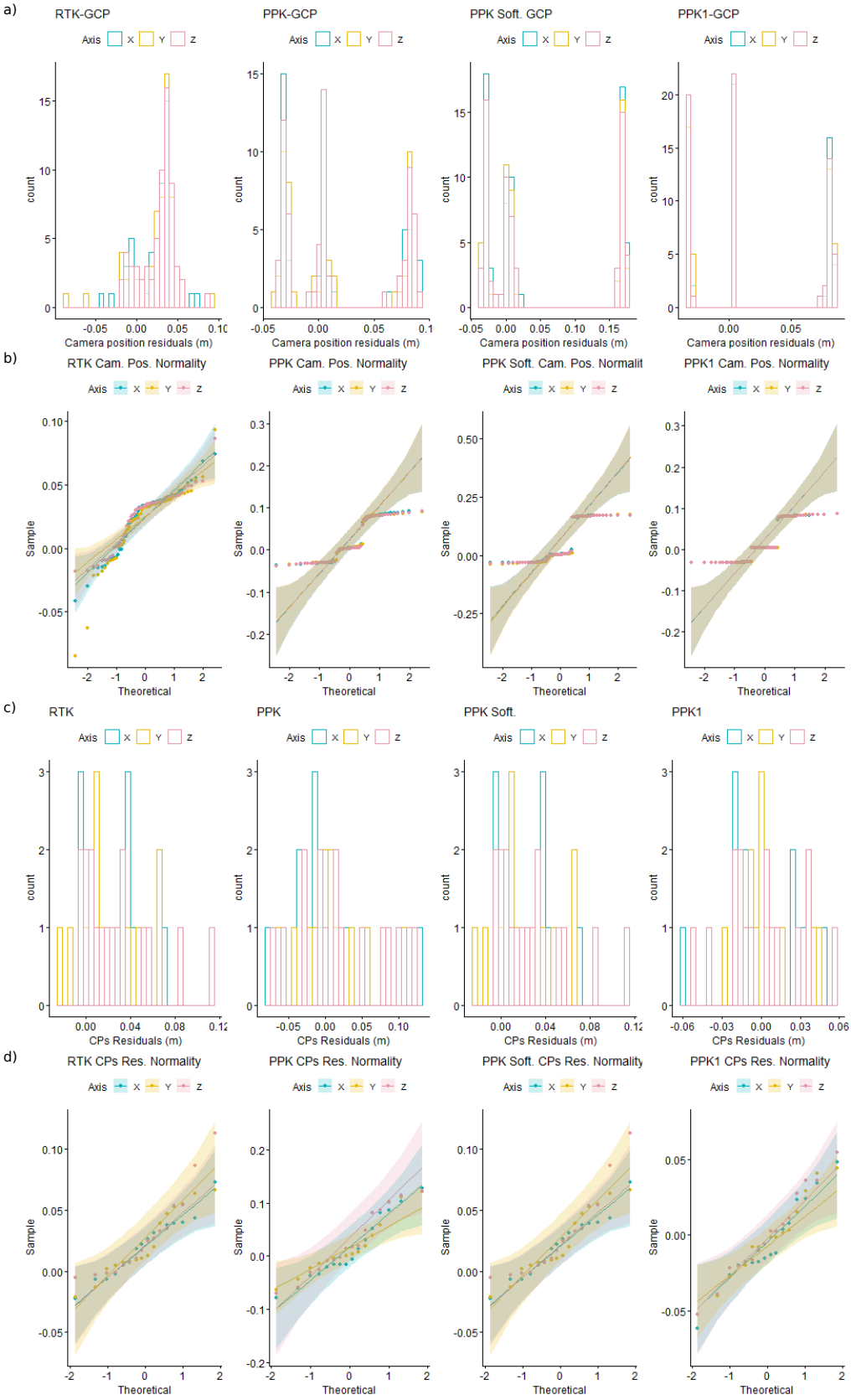

Figure A5. Results of 120 m terrain-following flight: (**a**) estimated camera position residual histograms, (**b**) camera position normality, (**c**) CP residuals, (**d**) CP residual normality plots.

References

1. Czapiewski, S. Assessment of the Applicability of UAV for the Creation of Digital Surface Model of a Small Peatland. *Front. Earth Sci.* **2022**, *10*, 834923. [CrossRef]
2. Brovkina, O.; Cienciala, E.; Surový, P.; Janata, P. Unmanned aerial vehicles (UAV) for assessment of qualitative classification of Norway spruce in temperate forest stands. *Geo-Spat. Inf. Sci.* **2018**, *21*, 12–20. [CrossRef]
3. Garg, P. *Unmanned Aerial Vehicles*; Mercury Learning and Information: Herndon, VA, USA, 2021.
4. Kovanič, L.; Blistan, P.; Rozložník, M.; Szabó, G. UAS RTK/PPK photogrammetry as a tool for mapping the urbanized landscape, creating thematic maps, situation plans and DEM. *Acta Montan. Slovaca* **2022**, *26*, 649–660. [CrossRef]
5. Padró, J.C.; Muñoz, F.J.; Planas, J.; Pons, X. Comparison of four UAV georeferencing methods for environmental monitoring purposes focusing on the combined use with airborne and satellite remote sensing platforms. *Int. J. Appl. Earth Obs. Geoinf.* **2019**, *75*, 130–140. [CrossRef]
6. Taddia, Y.; Stecchi, F.; Pellegrinelli, A. Coastal mapping using dji phantom 4 RTK in post-processing kinematic mode. *Drones* **2020**, *4*, 9. [CrossRef]
7. Erenoglu, R.C.; Erenoglu, O.; Arslan, N. Accuracy Assessment of Low Cost UAV Based City Modelling for Urban Planning. *Teh. Vjesn.—Tech. Gaz.* **2018**, *25*, 1708–1714. [CrossRef]
8. Zeybek, M.; Biçici, S. Road Distress Measurements Using UAV. *Türk Uzaktan Algılama CBS Dergisi* **2020**, *1*, 13–23.
9. Mancini, F.; Dubbini, M.; Gattelli, M.; Stecchi, F.; Fabbri, S.; Gabbianelli, G. Using unmanned aerial vehicles (UAV) for high-resolution reconstruction of topography: The structure from motion approach on coastal environments. *Remote Sens.* **2013**, *5*, 6880–6898. [CrossRef]
10. Carrera-Hernández, J.J.; Levresse, G.; Lacan, P. Is UAV-SfM surveying ready to replace traditional surveying techniques? *Int. J. Remote Sens.* **2020**, *41*, 4818–4835. [CrossRef]
11. Barry, P.; Coakley, R. Fiedl Accuracy Test of RPAS Photogrammetry. *Int. Arch. Photogramm. Remote Sens. Spat. Inf. Sci.* **2013**, *XL-1/W2*, 27–31. [CrossRef]
12. Furukawa, Y.; Ponce, J. Accurate, Dense, and Robust Multiview Stereopsis. *IEEE Trans. Pattern Anal. Mach. Intell.* **2010**, *32*, 1362–1376. [CrossRef] [PubMed]
13. Elkhrachy, I. 3D Structure from 2D Dimensional Images Using Structure from Motion Algorithms. *Sustainability* **2022**, *14*, 5399. [CrossRef]
14. Bemis, S.P.; Micklethwaite, S.; Turner, D.; James, M.R.; Akciz, S.; Thiele, S.T.; Bangash, H.A. Ground-based and UAV-Based photogrammetry: A multi-scale, high-resolution mapping tool for structural geology and paleoseismology. *J. Struct. Geol.* **2014**, *69*, 163–178. [CrossRef]
15. Westoby, M.; Brasington, J.; Glasser, N.; Hambrey, M.; Reynolds, J. 'Structure-from-Motion' photogrammetry: A low-cost, effective tool for geoscience applications. *Geomorphology* **2012**, *179*, 300–314. [CrossRef]
16. Eltner, A.; Hoffmeister, D.; Kaiser, A.; Karrasch, P.; Klingbeil, L.; Stöcker, C.; Rovere, A. *UAVs for the Environmental Sciences Methods and Applications*; wbg Academic: Darmstadt, Germany, 2022.
17. Nesbit, P.R.; Hubbard, S.M.; Hugenholtz, C.H. Direct Georeferencing UAV-SfM in High-Relief Topography: Accuracy Assessment and Alternative Ground Control Strategies along Steep Inaccessible Rock Slopes. *Remote Sens.* **2022**, *14*, 490. [CrossRef]
18. Zeybek, M.; Biçici, S. 3D Dense Reconstruction of Road Surface from UAV Images and Comparison of SfM Based Software Performance. *Turk. J. Remote Sens. GIS* **2021**, *2*, 96–105. [CrossRef]
19. Famiglietti, N.A.; Cecere, G.; Grasso, C.; Memmolo, A.; Vicari, A. A Test on the Potential of a Low Cost Unmanned Aerial Vehicle RTK/PPK Solution for Precision Positioning. *Sensors* **2021**, *21*, 3882. [CrossRef] [PubMed]
20. Zhang, H.; Aldana-Jague, E.; Clapuyt, F.; Wilken, F.; Vanacker, V.; Van Oost, K. Evaluating the potential of post-processing kinematic (PPK) georeferencing for UAV-based structure- from-motion (SfM) photogrammetry and surface change detection. *Earth Surf. Dyn.* **2019**, *7*, 807–827. [CrossRef]
21. Belloni, V.; Fugazza, D.; Di Rita, M. UAV-Based Glacier Monitoring: GNSS Kinematic Track Post-processing and Direct Georeferencing for Accurate Reconstructions in Challenging Environments. *Int. Arch. Photogramm. Remote Sens. Spat. Inf. Sci.* **2022**, *XLIII-B1-2*, 367–373. [CrossRef]
22. Bláha, M.; Eisenbeiss, H.; Grimm, D.; Limpach, P. DIRECT GEOREFERENCING OF UAVS. *Int. Arch. Photogramm. Remote Sens. Spat. Inf. Sci.* **2012**, *XXXVIII-1*, 131–136. [CrossRef]
23. Whitehead, K.; Hugenholtz, C.H. Applying ASPRS Accuracy Standards to Surveys from Small Unmanned Aircraft Systems (UAS). *Photogramm. Eng. Remote Sens.* **2015**, *81*, 787–793. [CrossRef]
24. Agüera-Vega, F.; Carvajal-Ramírez, F.; Martínez-Carricondo, P. Assessment of photogrammetric mapping accuracy based on variation ground control points number using unmanned aerial vehicle. *Measurement* **2017**, *98*, 221–227. [CrossRef]
25. James, M.R.; Robson, S.; D'Oleire-Oltmanns, S.; Niethammer, U. Optimising UAV topographic surveys processed with structure-from-motion: Ground control quality, quantity and bundle adjustment. *Geomorphology* **2017**, *280*, 51–66. [CrossRef]
26. Elkhrachy, I. Accuracy Assessment of Low-Cost Unmanned Aerial Vehicle (UAV) Photogrammetry. *Alex. Eng. J.* **2021**, *60*, 5579–5590. [CrossRef]
27. Iizuka, K.; Ogura, T.; Akiyama, Y.; Yamauchi, H.; Hashimoto, T.; Yamada, Y. Improving the 3D model accuracy with a post-processing kinematic (PPK) method for UAS surveys. *Geocarto Int.* **2022**, *37*, 4234–4254. [CrossRef]

28. Liu, X.; Lian, X.; Yang, W.; Wang, F.; Han, Y.; Zhang, Y. Accuracy Assessment of a UAV Direct Georeferencing Method and Impact of the Configuration of Ground Control Points. *Drones* **2022**, *6*, 30. [CrossRef]
29. Salas López, R.; Terrones Murga, R.E.; Silva-López, J.O.; Rojas-Briceño, N.B.; Gómez Fernández, D.; Oliva-Cruz, M.; Taddia, Y. Accuracy Assessment of Direct Georeferencing for Photogrammetric Applications Based on UAS-GNSS for High Andean Urban Environments. *Drones* **2022**, *6*, 388. [CrossRef]
30. Cirillo, D.; Cerritelli, F.; Agostini, S.; Bello, S.; Lavecchia, G.; Brozzetti, F. Integrating Post-Processing Kinematic (PPK)–Structure-from-Motion (SfM) with Unmanned Aerial Vehicle (UAV) Photogrammetry and Digital Field Mapping for Structural Geological Analysis. *ISPRS Int. J. Geo-Inf.* **2022**, *11*, 437. [CrossRef]
31. Zeybek, M. Accuracy assessment of direct georeferencing UAV images with onboard global navigation satellite system and comparison of CORS/RTK surveying methods. *Meas. Sci. Technol.* **2021**, *32*, 065402. [CrossRef]
32. Yildirim, Ö.; Mekik, Ç.; Bakici, S. TUSAGA-AKTİF CORS-TR Sisteminin Tapu ve Kadastro Genel Müdürlüğüne Katkıları. *Jeodezi Jeoinformasyon Derg.* **2011**, *104*, 134–139.
33. Estey, L.H.; Meertens, C.M. TEQC: The Multi-Purpose Toolkit for GPS/GLONASS Data. *GPS Solut.* **1999**, *3*, 42–49. [CrossRef]
34. Noll, C.E. The crustal dynamics data information system: A resource to support scientific analysis using space geodesy. *Adv. Space Res.* **2010**, *45*, 1421–1440. . [CrossRef]
35. Takasu, T.; Yasuda, A. Development of the low-cost RTK-GPS receiver with an open source program package RTKLIB. In Proceedings of the International Symposium on GPS/GNSS, Seogwipo-si, Republic of Korea, 4–6 November 2009; Volume 1, pp. 1–6.
36. Cleveland, W.S.; Grosse, E.; Shyu, W.M. Local Regression Models. In *Statistical Models in S*; Routledge: Oxfordshire, UK, 2017; Volume 35, pp. 309–376. [CrossRef]
37. R Core Team. *R: A Language and Environment for Statistical Computing*; R Foundation for Statistical Computing: Vienna, Austria, 2022.
38. Cleveland, W.S.; Devlin, S.J. Locally weighted regression: an approach to regression analysis by local fitting. *J. Am. Stat. Assoc.* **1988**, *83*, 596–610. [CrossRef]
39. Kuhn, M.; Johnson, K. *Applied Predictive Modeling*; Springer Nature: Berlin/Heidelberg, Germany, 2013; pp. 1–600. [CrossRef]
40. Arnold, T.; Kane, M.; Lewis, B.W. *Linear Smoothers*; CRC Press: Boca Raton, FL, USA, 2019; pp. 75–122. [CrossRef]
41. Ruppert, D.; Matteson, D.S. *Statistics and Data Analysis for Financial Engineering*; Springer Texts in Statistics; Springer: New York, NY, USA, 2015; pp. 75–122. [CrossRef]